Chaotic advection in the velocity field of leapfrogging vortex pairs

1995 J. Phys. A: Math. Gen. 28 2191

(http://iopscience.iop.org/0305-4470/28/8/013)

J. Phys. A: Math. Gen. 28 (1995) 2191–2216. Printed in the UK

Chaotic advection in the velocity field of leapfrogging vortex pairs

Á Péntek†, T Tél and Z Toroczkai‡
Institute for Theoretical Physics, Eötvös University, Puskin u. 5–7, H–1088 Budapest, Hungary

Received 21 November 1994

Abstract. The advection problem of passive tracer particles in the time-periodic velocity field of leapfrogging vortex pairs is investigated in the context of chaotic scattering. We numerically determine a few basic unstable periodic orbits of the tracer dynamics, and the non-attracting chaotic set responsible for the motion of particles injected in front of the vortex system. The latter consists of two parts: a hyperbolic component based on strongly unstable periodic orbits, and a non-hyperbolic component that is close to KAM surfaces. The invariant manifolds of the chaotic set are also plotted and their relevance for the particle dynamics is discussed. The tracer dynamics has one single dimensionless parameter: the energy of the vortex system. As a new phenomenon, we point out the existence of stable bounded trajectories between the vortex pairs at sufficiently large energies. A quantitative characterization of the tracer dynamics in terms of *the so-called free energy function is given and the multifractal spectrum of Lyapunov exponents*, the escape rate and other characteristics of the transient chaotic motion are determined.

1. Introduction

The advection of passive tracer particles in non-stationary fluid flows has attracted recent interest since particle motion is generally more complex than the underlying velocity field [1–4]. Chaotic advection provides an appealing application of the chaos concept in a phenomenon observable by naked eyes. The connection with dynamical system theory is especially strong in two-dimensional incompressible flows where the latter property implies the Hamiltonian character of the particle motion.

The investigation of chaotic advection in viscid flows [5–12] led to a better understanding of mixing in closed containers. The associated particle dynamics is then characterized by a bounded phase space. Advection in open flows [13–19] has the novel feature of having unbounded particle trajectories. Because of the asymptotic simplicity of the motion, the particle dynamics can be considered as a type of scattering process. In fact, the motion in time periodic flows can be chaotic, like, for example, that of particles coming close to the obstacle in a von Kármán vortex street [17–19]. Knowledge accumulated in the field of chaotic scattering [20–22] has turned out to be a powerful tool to describe this phenomenon.

Chaotic advection in inviscid fluids typically occurs in the velocity field of interacting vortices [23–26]. In systems of a few interacting point vortices one often finds *both* bounded

† Permanent address: Institute for Pure and Applied Physical Sciences, University of California at San Diego, La Jolla, California 92093-0075, USA.
‡ Permanent address: Department of Physics, Virginia Polytechnic Institute and State University, Blacksburg, Virginia 24061, USA.

0305-4470/95/082191+26$19.50

and unbounded tracer trajectories. Previous studies had certain difficulties with interpreting chaos associated with the unbounded motion. The aim of this paper is to show that this difficulty can be overcome by using recent results of the theory of chaotic scattering, or more generally of transient chaos [27].

In particular, we point out that for the scattering tracer dynamics there exists an *infinity of unstable periodic orbits. In fact, the number of periodic orbits increases exponentially* with their period. Periodic orbits provide a backbone for this dynamics in the sense that the particle might stay close to a periodic orbit for a while, then leave it and come into the vicinity of another one, and so on before escaping to infinity. The union of all the bounded unstable periodic orbits together with their heteroclinic and homoclinic connections forms a *non-attracting chaotic set.* The chaotic set possesses a *stable manifold* along which trajectories can reach the set itself. It is essential for the understanding of the advection problem that the stable manifold is an object of measure zero and provides a *fractal* foliation of the space. This is why a particle has zero probability of being trapped forever by a periodic orbit, or by the entire chaotic set. Although the chaotic set itself is also a fractal, there exists a *natural measure* on it. Chaotic characteristics, like, for example, the average Lyapunov exponent, of trajectories coming close to the set can be computed by taking averages with respect to this natural measure [27].

We consider a simplified model of the so-called leapfrogging motion of two vortex rings. If the rings have the same sense of rotation, they travel in the same direction. In cases when the rings move along the same axis, the rear vortex ring attempts to pass through the front one. The leading ring then widens due to the mutual interaction and travels more slowly. Simultaneously, the other ring shrinks, travels faster and penetrates the first one. The process can then be repeated again and again. Recently Shariff and coworkers [28, 29] have performed a detailed simulation of particle trajectories in the field of leapfrogging vortex rings in viscid fluids and found good agreement with smoke visualization pictures reported in experiments [30]. We shall study the two-dimensional analogue of this process in an inviscid flow: advection in the field of two pairs of ideal point vortices of the same strength exhibiting leapfrogging motion. It will turn out that this simple model faithfully describes the qualitative features of the advection in the field of three-dimensional leapfrogging vortex rings. At the same time its simplicity allows for precise calculations and a detailed investigation of the parameter dependence. Alternatively, the advection problem induced by two leapfrogging vortex pairs can also be considered as that induced by two vortices moving in front of a wall lying on the symmetry axis of the original problem [31–33].

It is known that the integrability of the advection in the field of autonomous point vortices depends on the number of vortices and on the type of solid boundaries [34–37]. Let us consider cases without external flows. In unlimited space, the tracer dynamics is always integrable if the number of vortices is at most two. With more vortices the tracer dynamics is non-integrable even if the vortex motion itself is periodic or quasiperiodic, like, for example, in the case of three vortices [23, 35]. When the presence of solid boundaries breaks either the rotational or translational symmetry, the minimum number of vortices leading to non-integrability is decreased by one [36]. If both symmetries are broken, as in a general closed domain, even the advection induced by a single vortex, exhibiting periodic motion, becomes non-integrable [36, 37]. In our problem a straight line boundary breaks the rotational symmetry and thus the advection generated by two vortices is already non-integrable.

The paper is organized as follows. In section 2 the leapfrogging motion of two vortex pairs is described. Analytical results for the period and the average velocity are given in the

appendix. Section 3 is devoted to the discussion of the corresponding advection problem. We point out that the phenomenon is especially simple in a frame comoving with the centre of mass of the vortex pairs and is then invariant under certain symmetry operations. A few basic unstable periodic orbits are also determined. Next, in section 4, we turn to the investigation of the chaotic set responsible for the scattering tracer motion, and its invariant manifolds. We show that around the vortex centres there is always a region that cannot be reached by trajectories coming from outside and that region is bounded by a kind of KAM torus. Thus, because of the mere presence of the vortices, the advection dynamics is never purely hyperbolic. It has one single dimensionless parameter: the energy of the vortex system. The dependence of the advection on this energy is briefly discussed in section 5. As a new phenomenon, we point out the existence of *stable* bounded trajectories *between* the vortex pairs at sufficiently large energies. The region of bounded motion outside of the vortex cores is separated by typical KAM surfaces. Simultaneously bounded chaos inside these KAM tori becomes easily observable. In the limit of very large energies the advection can be considered as a slight time-dependent perturbation of the advection in the field of a single vortex pair. A quantitative characterization of the tracer dynamics in terms of the so-called free energy function is given in section 6. It is emphasized that most of the important characteristic numbers can be extracted from this single function. The paper is concluded in section 7 with the discussion of some open problems.

2. Leapfrogging motion of two vortex pairs

The dynamics of point vortices in two-dimensional flows of ideal incompressible fluids, or of parallel vortex lines in three-dimensional ones, is a classical field of hydrodynamics. It was recognized by Helmholtz and other researchers at the end of the last century [31–33] that the equations of motion of a system of such vortices can be cast into a canonical form. The Hamiltonian of n interacting vortices reads as

$$H(\{x_i, y_i\}) = -\frac{1}{\pi}\sum_{i<j}\kappa_i\kappa_j \ln r_{i,j} \tag{1}$$

where (x_i, y_i) stands for the position of vortex i $(i = 1, \ldots, n)$ of strength κ_i in the (x, y) plane, and $r_{i,j}$ is the distance between vortices i and j. The value E of the Hamiltonian is constant in time and can thus be called the energy of the vortex system. The equations of motion are of the Hamiltonian form [31–33]

$$\kappa_i\dot{x}_i = \frac{\partial H}{\partial y_i} \qquad \kappa_i\dot{y}_i = -\frac{\partial H}{\partial x_i}\,. \tag{2}$$

Note the analogy with the canonical equations of point mechanics when one identifies, for example, x and κy with the generalized coordinates and momenta, respectively. The equations can be rendered dimensionless by means of the transformations

$$(x, y) \to (lx, ly) \qquad t \to \frac{\pi l^2}{\kappa}t \qquad H \to \frac{\kappa^2}{2\pi}H \tag{3}$$

where κ is a preselected vortex strength, and l denotes a characteristic length scale.

It is known [34–41] that the motion of four or more vortices is, in general, chaotic. In this paper we study a case where the dynamics of four vortices is integrable: the motion of two vortex pairs of equal strengths that move in the same direction along a common symmetry axis perpendicular to the extension of both pairs (see figure 1). When interpreting the problem as the motion of two point vortices in front of a wall, the vortices in the lower

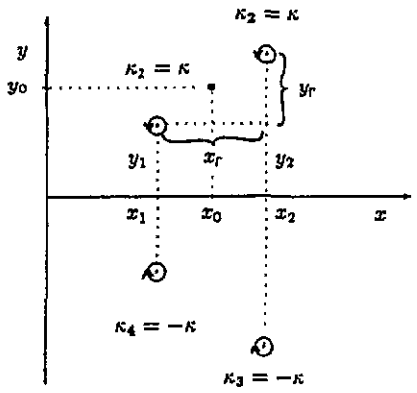

Figure 1. Geometry of two leapfrogging vortex pairs. Relative and centre-of-mass coordinates are also indicated.

half-plane appear as 'mirror' vortices introduced in the same spirit as mirror charges are in electrostatics. We shall call this version the symmetry-reduced problem.

The Hamiltonian of the system defined in figure 1 reads as

$$H(x_1, x_2, y_1, y_2) = \frac{\kappa^2}{2\pi}(-2\ln r_{1,2} + 2\ln r_{2,4} + \ln r_{1,4} + \ln r_{2,3})$$
$$= \frac{\kappa^2}{2\pi}\ln\left(4y_1y_2\frac{(x_1-x_2)^2+(y_1+y_2)^2}{(x_1-x_2)^2+(y_1-y_2)^2}\right) = E\,. \tag{4}$$

The extra factor $\frac{1}{2}$ missing in (1) appears here because the mirror vortex coordinates are not independent variables in the symmetry-reduced problem [42]. Since the centre-of-mass coordinate

$$x_0 \equiv (x_1 + x_2)/2 \tag{5}$$

does not appear in H (is a cyclic variable), the conjugate variable

$$2y_0 \equiv (y_1 + y_2) = \text{constant} \tag{6}$$

is conserved during the motion. $2y_0$ can be considered as the average width of the vortex pairs. In what follows we choose $2y_0$ as the characteristic length

$$l = 2y_0 \tag{7}$$

and rescale the problem according to (3). It is then worth using, besides the centre-of-mass coordinates, the relative variables

$$x_r \equiv x_2 - x_1 \qquad y_r \equiv y_2 - y_1. \tag{8}$$

The energy conservation (4) provides us with the explicit form of trajectories in the relative coordinates as

$$\frac{1}{1-y_r^2} - \frac{1}{1+x_r^2} = \mathrm{e}^{-E}\,. \tag{9}$$

Bounded trajectories are present for energy values $E > E_s \equiv 0$ where no real solution y_r exists for $x_r \to \infty$. The energy $E_s = 0$ corresponds to a separatrix in phase space lying on the boundary between regions occupied by open and closed trajectories (figure 2). The latter correspond to *strictly periodic* motions of the vortex pairs, called leapfrogging [28–30]. In the remainder of the paper we concentrate on this region, $E > 0$.

Because of the conservation of y_0, there are only three independent dynamical variables left. Since the Hamiltonian depends on x_r and y_r only, their equations of motion form a

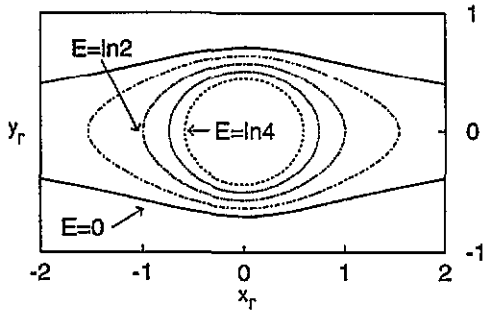

Figure 2. Vortex trajectories in relative coordinates (x_r, y_r) for different energy values $E = n \ln 2$ with $n = 0, 0.5, 1, 1.5, 2$. Dimensionless variables defined by (3), (7) are used. $E = 0$ is the separatrix (full curve) on the boundary between closed and open trajectories.

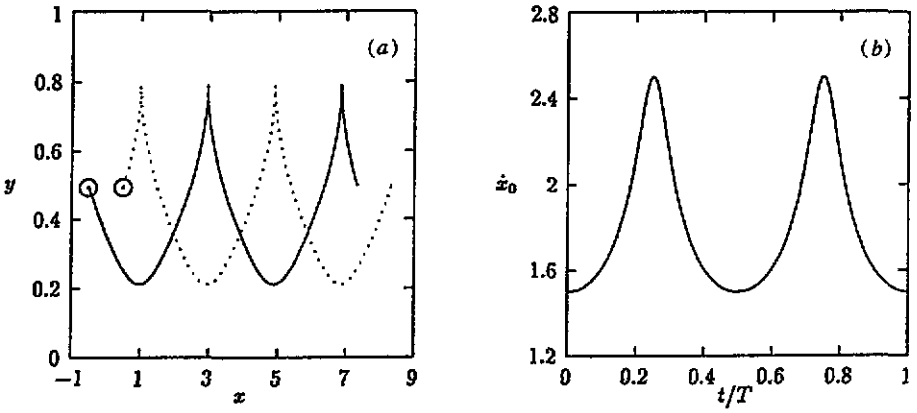

Figure 3. Leapfrogging motion for $E = \ln 2$. (*a*) Cycloid shaped trajectories of the two upper vortices in the standing reference frame. The initial condition taken is $x_{1(2)} = -(+)0.5$, $y_{1(2)} = 0.5$. (*b*) The velocity of the centre-of-mass coordinate $v_0(t) = \dot{x}_0(t)$ in the standing reference frame. The period and the average velocity are $T = 2.16$ and $\bar{v}_0 = 1.83$, respectively.

closed system (explicitly given in the appendix) that can be solved by direct numerical integrations. Figure 3(*a*) shows the cycloid shaped trajectories of the vortices in the standing reference frame. After solving for the relative motion, $x_0(t)$ is obtained by simple quadrature. We emphasize that the velocity $v_0(t) \equiv \dot{x}_0(t)$ of the centre of mass along the x-axis is *not* constant in contrast to the usual two-body problem. Its average value $\bar{v}_0$ (see figure 3(*b*)) is close to 2 for a broad range of energies.

The period $T(E)$ and the average velocity $\bar{v}_0(E)$ of the motion depends solely on the energy and can be expressed in terms of elliptic integrals (see the appendix). The dimensionless energy value belonging to the plots of figure 3 is $E = \ln 2 = 0.693$ that we shall keep as an illustrative case also in the next two sections.

3. The advection problem

An isolated vortex of strength κ generates at distance r from its centre a circulational flow with a velocity field proportional in modulus to κ/r. The stream function $\psi(x, y)$, whose cross derivatives yield the velocity components v_x and v_y [31, 32], is $-(\kappa/\pi) \ln r$. In the system of n vortices these contributions are superimposed, and one obtains

$$\psi(x, y, t) = -\sum_j \frac{\kappa_j}{\pi} \ln r_j(t) \tag{10}$$

where $r_j(t)$ stands for the distance of point (x, y) from vortex j. Because the vortices follow their own dynamics, the distances $r_j(t)$, and consequently also the streamfunction, are time-dependent. The velocity components at a given point (x, y) and time t are then obtained as

$$v_x(x, y, t) = \frac{\partial \psi}{\partial y} \qquad v_y(x, y, t) = -\frac{\partial \psi}{\partial x}. \tag{11}$$

A passively advected particle simply follows the local velocity field, therefore, its equations of motion, sometimes called the Lagrangian dynamics, are given by

$$\dot{x} = \frac{\partial \psi(x, y, t)}{\partial y} \qquad \dot{y} = -\frac{\partial \psi(x, y, t)}{\partial x}. \tag{12}$$

Note again the canonical character of the problem in which the streamfunction plays the role of the Hamiltonian.

The difference compared with the vortex motion is that the dynamics is now non-autonomous. The advection problem can be cast into a dimensionless form via transformations similar to (3). For the streamfunction we shall use the rescaling $\psi \to (\kappa/\pi)\psi$.

In the particular case of the leapfrogging vortex pairs of equal strength (i.e. $\kappa_1 = \kappa_2 = -\kappa_3 = -\kappa_4 \equiv \kappa$) the dimensionless streamfunction (10) takes the form (cf figure 1)

$$\psi(x, y, t) = \ln\left(\frac{r_3(t)\, r_4(t)}{r_1(t)\, r_2(t)}\right) \tag{13}$$

where

$$r^2_{1(2)}(t) = [x - x_{1(2)}(t)]^2 + [y - y_{1(2)}(t)]^2 \tag{14}$$

$$r^2_{3(4)}(t) = [x - x_{2(1)}(t)]^2 + [y + y_{2(1)}(t)]^2 \tag{15}$$

with $x_{1,2}(t)$ and $y_{1,2}(t)$ being the solutions of the vortex problem studied in the previous section. Due to the periodicity of the vortex motion and the nonlinearity of (12), the motion of advected particles can be chaotic.

It is particularly convenient to use a reference frame whose origin is comoving with the point $(x_0(t), y = 0)$ along the x-axis. We shall call this frame the centre-of-mass system (CMS) of the symmetry-reduced problem. The streamfunction valid in the CMS is

$$\psi_{\mathrm{CMS}}(x, y, t) = \psi(x, y, t) - v_0(t)y \tag{16}$$

where vortex coordinates $x_2 = -x_1 = x_r/2$ relative to the CMS have to be used.

Due to the subtraction of the velocity $v_0(t)$ from the field generated by (13)–(15), two *instantaneous* stagnation points $P_\pm$ are created in the CMS along the x-axis. Figure 4 shows the instantaneous streamlines and stagnation points at two different instants of time $t = 0$ and $t = T/4$. We use the convention that $t = 0$ corresponds to the configuration when the width of both vortex pairs is the same ($y_1 = y_2 = y_0$). The stagnation points exhibit a periodic motion of period $T/2$. The particles situated at these stagnation points have zero velocities and cannot follow the periodic motion of the geometrical points $P_\pm$. The motion of the stagnation points, therefore, does *not* correspond to a periodic orbit of the advection dynamics.

Both the advection dynamics and the motion in the frozen streamlines of figure 4 share some basic properties. The $y = 0$ line is an invariant curve, the motion restricted to it is *dissipative* and possesses two fixed points: an attractor and a repellor. This is not surprising since the dynamics on invariant surfaces of Hamiltonian systems are in general not area preserving [43]. In the instantaneous streamline pattern the two fixed points are the two

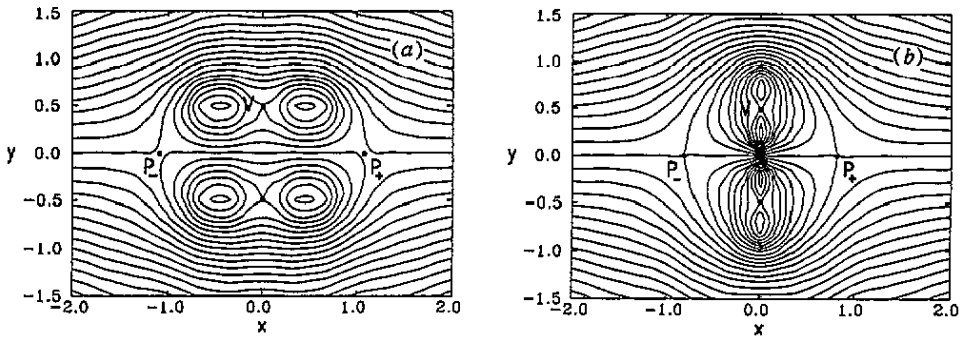

Figure 4. Instantaneous streamlines in the CMS frame for $E = \ln 2$ at (*a*) $t = 0$ and (*b*) $T/4$. These configurations correspond to extreme positions of the two stagnation points $P_\pm$. V is the central stagnation point at half-way between the vortices.

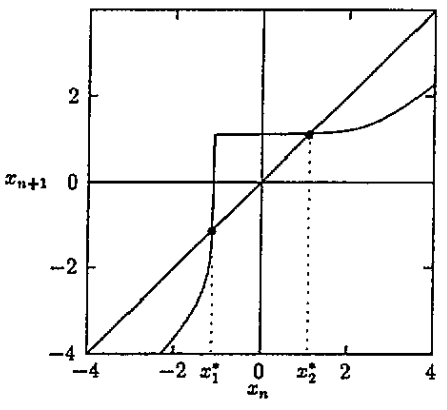

Figure 5. Stroboscopic map (taken at multiples of $T/2$) of the dynamics restricted to the $y = 0$ axis of the CMS for $E = \ln 2$. Observe the unstable and stable fixed points at $x^*_{1(2)} = \mp 1.114$ with slopes 34 and $\frac{1}{34}$, respectively corresponding to two hyperbolic period-1 orbits $P_{1(2)}$ shown in figures 8–10.

stagnation points $P_{+(-)}$, while in the *advection* problem they are two other orbits $P_{2(1)}$. The latter correspond the *truly periodic motions* of particles inside the region in which the geometrical points $P_{+(-)}$ are oscillating.

In order to specify the position of the periodic orbits $P_{1(2)}$ on the x-axis, we numerically solved the dynamics restricted to $y = 0$ in the CMS. In a similar spirit to [13], we determined a one-dimensional return map by computing the x-coordinate after a time difference of $T/2$. The result obtained at $t = 0 \bmod T/2$ for $E = \ln 2$ is given in figure 5. It clearly shows the existence of an attractor and a repellor point at $x_2^* = 1.114$ and $x_1^* = -1.114$, respectively. Note the rather large (small) value of the slope at the repellor (attractor) point. Being embedded into the (x, y) plane, these invariant points appear to be hyperbolic on the stroboscopic map of the full Hamiltonian dynamics. Thus the larger eigenvalue of the periodic orbit P_1 is the same number as the slope $\Lambda = 34$ of the map at x_1^*.

In order to study periodic orbits outside the x-axis, it is worth taking into account the symmetry properties of the velocity field.

(i) The obvious invariance against the exchange of the vortex centres implies the periodicity of the velocity field with $T/2$ where T is the period of the vortex motion. Thus it is worth defining a two-dimensional stroboscopic map for the advection problem by taking snapshots with a time difference $T/2$.

(ii) In the CMS a stronger symmetry also holds when applying the transformations:

$$(a)\ x_{1(2)} \to x_{2(1)} \qquad \text{or} \qquad (b)\ y_{1(2)} \to y_{2(1)} \tag{17}$$

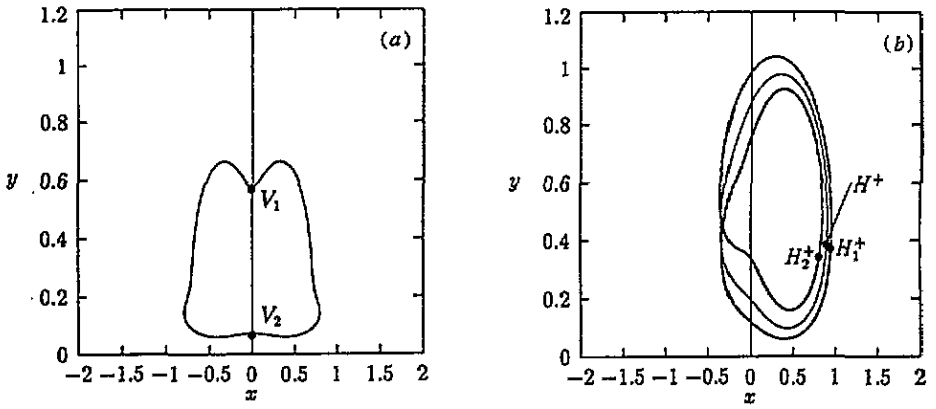

Figure 6. A few basic periodic orbits of the symmetry-reduced problem in the CMS. (*a*) An axisymmetric period-2 orbit. Coordinates on the stroboscopic map taken at $t = 0 \bmod T/2$ are $V_1(0, 0.575)$ and $V_2(0, 071)$. (*b*) Asymmetric periodic orbits: a period-1 orbit and a period-2 orbit around it. They generate points $H^+(0.902, 0.388)$, and $H_1^+(0.951, 0.375)$ and $H_2^+(0.814, 0.346)$, respectively, on the stroboscopic map.

together with changing the sign of the x-coordinate of the tracer particle ($x \to -x$) in both cases. Because of the time-reversal symmetry of the vortex dynamics and the symmetry of the graph of the CMS velocity (figure 3(*a*)), the exchange (*a*) and (*b*) of the vortices connects configurations taken at some time t and $T/2 - t$. Thus the velocity field fulfils the relation

$$v_x(x, y, t) = v_x(-x, y, T/2 - t) \tag{18}$$

$$v_y(x, y, t) = -v_y(-x, y, T/2 - t) \tag{19}$$

for any $0 < t < T/2$. As a consequence, a trajectory starting from some point (x_{in}, y_{in}) at time t will have the same shape as the time-reversed trajectory started from $(-x_{in}, y_{in})$ at $T/2 - t$. These trajectories will be mirror images of each other with respect to the y-axis. This implies that periodic orbits are either axisymmetric themselves or appear in pairs that are mirror images with respect to the y-axis. At times $t = 0, T/4 \pmod{T/2}$ holds in addition that if a periodic orbit starts from (x_{in}, y_{in}), its mirror image orbit will start from $(-x_{in}, y_{in})$. This property makes the use of stroboscopic maps taken at $t = 0$ or $T/4 \pmod{T/2}$ especially convenient.

It is worth mentioning that these symmetries are due to the assumption that both vortex pairs are of equal strength ($\kappa_1 = \kappa_2 = \kappa$). In a model with different strength they would not be present.

A few basic periodic orbits obtained numerically are shown in figure 6. The axisymmetric orbit (figure 6(*a*)) is of period T. Therefore it generates two points V_1 and V_2 on the stroboscopic map taken with a time difference of $T/2$. This axisymmetric orbit is unstable, too, its eigenvalue is 8. We have also found a pair of asymmetric orbits of period $T/2$ (figure 6(*b*), thin curve) defining fixed points $H^{\pm}$ on the stroboscopic map. These unstable trajectories stay mainly in one of the half-planes. Around them, there exist similar two-loop trajectories of period T (figure 6(*b*), full curve) each generating two points $H_{1,2}^{+(-)}$ on the stroboscopic map.

Typical particle trajectories in the CMS are plotted in figure 7. Particles injected outside of the vortex system escape to infinity (figure 7(*a*)–(*d*)). Some of them follow a simple path (figure 7(*a*)) but some others exhibit a complicated motion before escaping. Long-lasting

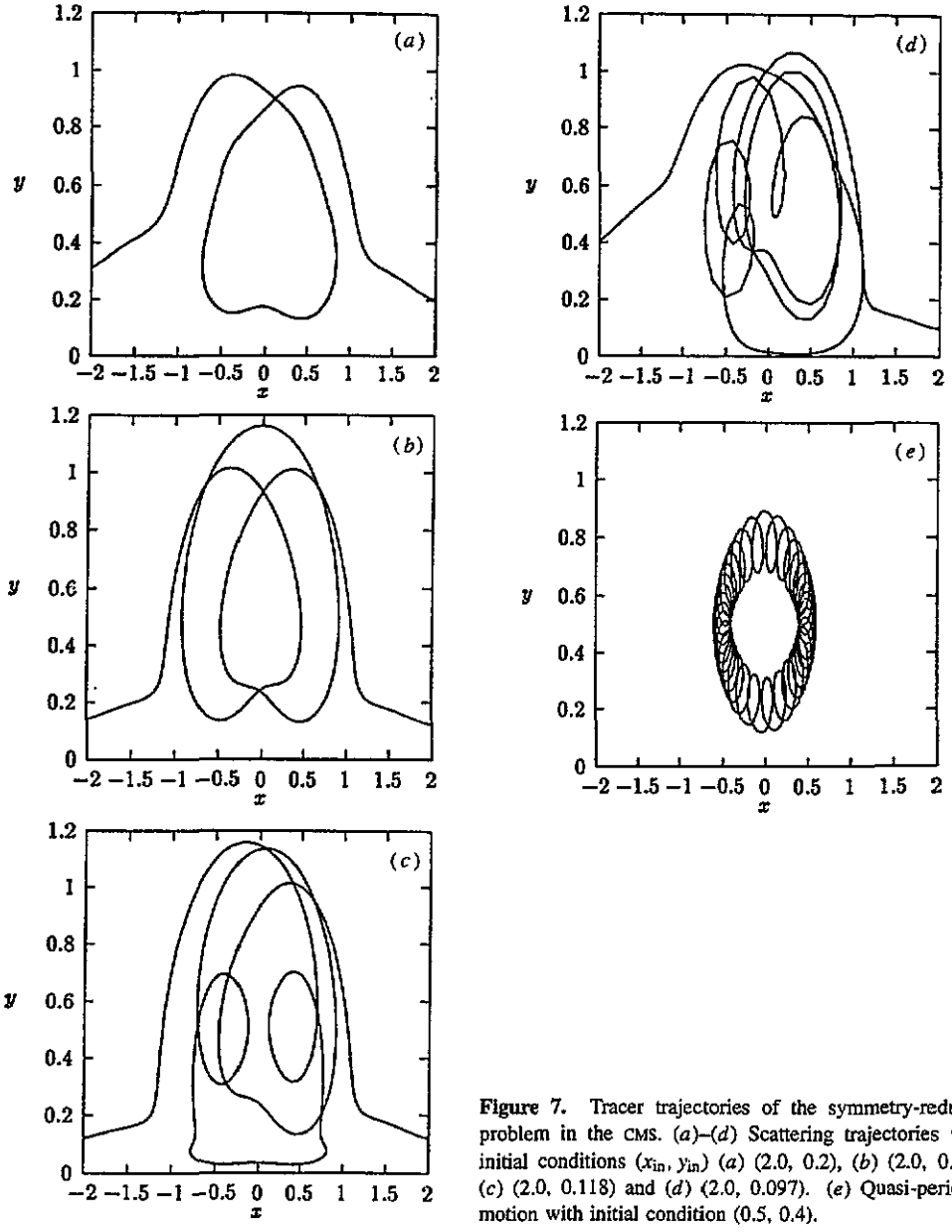

Figure 7. Tracer trajectories of the symmetry-reduced problem in the CMS. (*a*)–(*d*) Scattering trajectories with initial conditions (x_{in}, y_{in}) (*a*) (2.0, 0.2), (*b*) (2.0, 0.12), (*c*) (2.0, 0.118) and (*d*) (2.0, 0.097). (*e*) Quasi-periodic motion with initial condition (0.5, 0.4).

chaotic motion between the vortex pairs can be considered as a random walk among unstable periodic orbits. Thus, for example, on figure 7(*a*) and (*b*) parts of the periodic orbits shown in figures 6(*a*) and (*b*) can, respectively, be seen. Particles put initially very close to one of the vortices do not escape and exhibit a periodic or quasi periodic motion around the vortex (figure 7(*e*)). Thus, depending on the initial conditions, particle trajectories can be both bounded and unbounded. Correspondingly, the full invariant set can be decomposed into a part responsible for the bounded motion and into another one accessible by trajectories coming in from infinity.

Our numerical experience indicates that at modest values of the vortex energy, $E \leqslant 0.9$, chaotic sets responsible for bounded chaotic motion (e.g. in the vicinity of one of the vortices) must be very small. Therefore we shall concentrate in what follows on chaotic sets connected with scattering trajectories coming in from infinity.

4. Invariant manifolds of periodic orbits, and the chaotic set

Let us consider the non-trivial manifolds of the fixed points P_1 and P_2 (denoted by W_1^s and W_2^u, respectively) discussed in the previous section producing several heteroclinic intersections. Taking the stroboscopic section just at $t = 0$ or $t = T/4$ (mod $T/2$), the manifolds W_1^s and W_2^u are mirror images of each other with respect to the y-axis.

To help understanding, the schematic figure 8 illustrates the most important topological features of the manifolds' intersection pattern. One can define an *interaction region* S bounded by segment P_2O of W_2^u and segment P_1O of W_1^s, where O is the first heteroclinic intersection point along both manifolds. Lobes formed by W_2^u and the boundary of the interaction region are denoted inside (outside) S by E_i (D_i) for $i > 0$. The direct Lagrangian dynamics transforms each lobe E_i (D_i) after $t = T/2$ onto E_{i+1} (D_{i+1}). This rule extends the definition of the lobes for $i \leqslant 0$. We use the convention that the first (last) lobe that lies inside the interaction region has label $i = 0$. Due to the Hamiltonian nature of the problem the area of all the lobes should be equal.

A direct numerical computation of the manifolds W_1^s and W_2^u shows that their actual form is much more complicated than those depicted in the schematic diagram of figure 8. Figure 9(a) displays the first branches of W_1^s and W_2^u while the full unstable manifold is shown in figure 9(b). The complex form of the lobes, and so their non-trivial intersections, can be understood by also taking into account the axisymmetric unstable periodic orbit (V_1 and V_2 on the stroboscopic map). It plays an essential role due to its relatively high eigenvalue. The first lobe E_0 comes close to V_1, V_2 and becomes strongly stretched along their unstable manifolds. Because of its strange shape, lobe E_0 intersects D_0 in six points, which also implies that each lobe E_i has the same number of intersections with D_i. A high-resolution investigation indicates the splitting of lobe E_1 into many fine strips (not only in two as for E_0) due to the presence of other periodic orbits causing altogether 24 intersections with D_0 (not shown).

It is instructive to follow how the content of the lobes is evolving, i.e. the so-called lobe dynamics [4, 9, 24, 44]. One can observe that points from $E_i \cap D_j$ spend time $(i-j+1)\,T/2$ inside S. In particular, points escaping the interaction region after $T/2$, independently of when they entered S, lie in D_0. Those spending just one time unit $T/2$ in the interaction region lie in $E_0 \cap D_0$. The escape rate α is defined as the exponential decay rate of the time delay statistics, i.e. of the probability to find trajectories spending a time longer than $nT/2$ trapped by the vortex system. Assuming the validity of this exponential form for any time (that does not hold exactly in general), we can estimate the escape rate as the logarithm of the area ratio between S and $S - D_0$. In our case this yields the approximate value $\alpha = 0.34$.

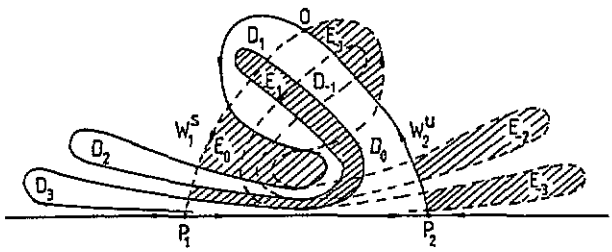

Figure 8. Schematic diagram of the stable and unstable manifolds W_1^s and W_2^u of the fixed points P_1 and P_2 in the CMS, respectively, on the stroboscopic map. Note that in the full problem the invariant manifolds have other branches that can be obtained as the mirror images of W_1^s and W_2^u taken with respect to the x-axis.

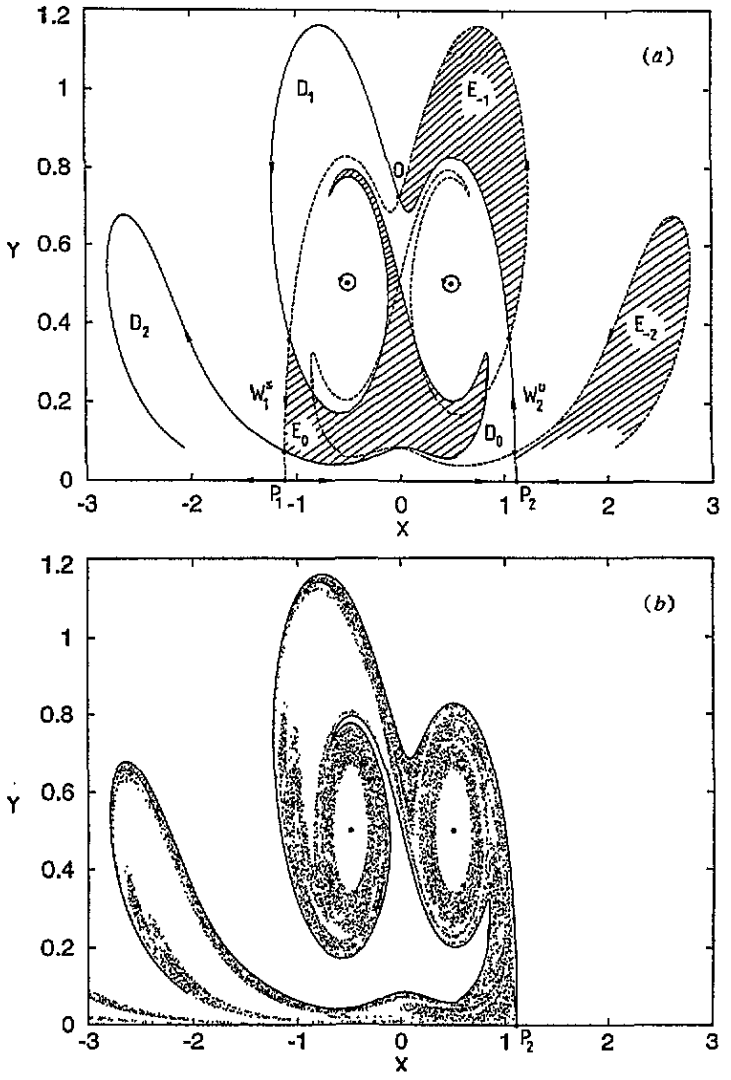

Figure 9. The non-trivial manifolds of $P_{1,2}$ obtained numerically in the CMS at $t = 0 \bmod T/2$. (*a*) The first branches of the manifolds W_1^s and W_2^u. (*b*) The full unstable manifold W_2^u. The corresponding stable manifold W_1^u is just its mirror image with respect to the y-axis. The vortex centres are marked by full circles.

The heteroclinic intersections of the manifolds W_1^s and W_2^u implies the existence of a Smale horseshoe and a chaotic set in the system. Correspondingly, unbounded particle trajectories might come close to this set and exhibit chaotic features. Since, however, the set is globally not attracting (that would contradict the Hamiltonian character) this chaos is necessarily of transient type restricted to finite time-scales [27]. In other words, particles can be trapped by the vortex system but, with the exception of a set of initial conditions of measure zero, sooner or later they escape. The union of the heteroclinic points between W_1^s and W_2^u is a good approximation to the non-attracting chaotic set existing in the unbounded part of the phase space (unstable periodic orbits also belong to the set but they are close to the heteroclinic orbits and thus do not change the geometrical appearance).

The numerical construction of this chaotic set is very efficient by means of a method called the PIM triple algorithm. This method introduced by Nusse and Yorke [45] yields a long sequence of very short pieces of trajectories (called a *saddle-straddle orbit*) assumed to straddle a true orbit on the chaotic set. The algorithm is the following. Take a segment which crosses the stable manifold of the set, and iterate a number n of points distributed evenly on this segment. Measure their time delay, i.e. the time the different trajectories spend in the interaction region. Three neighbouring initial points with the property that the midpoint has the longest time delay are called a *proper interior maximum* (PIM) triple. Trajectories starting in the sidepoints of a PIM triple obviously straddle a filament of the chaotic set's stable manifold. Choose a PIM triple and, by distributing the same number n of points on it as originally, find a shorter one. Iterate this refinement until the length of the last PIM triple becomes shorter than a preselected value $\epsilon_1 \ll 1$. Then, follow the evolution of the sidepoints of such a PIM triple as long as the distance between the trajectories is shorter than another preselected value $\epsilon_2 \ll 1$ ($\epsilon_2 > \epsilon_1$). Next, start searching for a new PIM triple on the segment connecting the endpoints of these trajectories, and repeat the whole procedure again and again. The generated series of segments of length shorter than ϵ_1 will cover the chaotic set in a coarse-grained description of resolution ϵ_1, and the pieces of trajectories starting in the sidepoints of the narrowest PIM triple straddle an orbit on the chaotic set with accuracy ϵ_2. In order to avoid an overaccumulation of points on the KAM surfaces, we have used a slightly modified version of the original algorithm by choosing PIM triples at random, as worked out for generic Hamiltonian systems in [46].

The chaotic set plotted in this way is the invariant set felt by scattering trajectories (figure 10). It can clearly be divided into two parts. One of them contains structures of double fractal character that are approximately direct products of two Cantor sets. The deltoidal forms along the symmetry axis at the height of 0.6, and the ones at the two sides

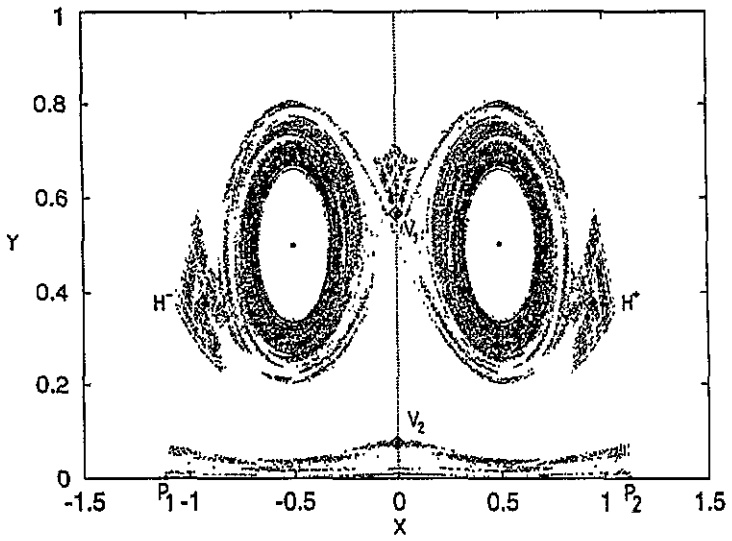

Figure 10. The chaotic set of the symmetry-reduced problem in the CMS obtained at $t = 0 \bmod T/2$ by means of the PIM triple algorithm. The parameters of the algorithm have been $n = 10$, $\epsilon_1 = 10^{-6}$ and $\epsilon_2 = 10^{-4}$ (see text). Notice the direct product structure of the hyperbolic part containing the main periodic points ($P_{1,2}$, $V_{1,2}$, $H^{+,-}$) and the dense spirals around the vortex cores forming the non-hyperbolic part. Note that the periodic points $P_{1,2}$ are the extremal points of the set. The vortex centres are marked by full circles.

of the plot at the height of 0.4 are of this type. The two latter forms are mapped onto themselves under the Lagrangian dynamics after a time $T/2$. The elongated structure on the bottom of the figure is the image of the deltoidal form on the symmetry axis but its direct product structure is less striking because of the strong stretching along the x-axis. These four blocks can be considered to be the *hyperbolic* component of the non-attracting chaotic set as they contain the strongly hyperbolic periodic orbits (like e.g. $P_{1,2}, V_{1,2}$ or $H^{\pm}$) of the dynamics. The existence of such structures is well known for purely hyperbolic chaotic scattering systems [21, 22].

In order to understand the spiral-like patterns, we first mention that the white ellipsoidal regions around the vortices are obviously not accessible by scattering trajectories. These are the regions where the effect of one vortex is more pronounced than that of any other one and can therefore be called the *vortex core* for the Lagrangian dynamics. Inside this core the effect of the other vortices is just a weak perturbation, and the conditions of the KAM theory [47] are thus fulfilled. Tracer particles put into this regime can also exhibit bounded chaotic motion but the size of such chaotic regions inside the core is obviously very small at energy values less than $E \simeq 0.9$. The majority of trajectories will thus be quasiperiodic as illustrated by figure 7(*e*). The boundary of the core is a KAM torus. At first sight it appears rather smooth but an enlargement of the torus surface (plotted for convenience in polar coordinates in figure 11) shows that by approaching it from outside complicated structures appear with little islands and chaotic regions intertwined. It is worth mentioning that such tori surrounding the vortices are present in the advection induced by any number of vortices [48]. They provide a region where the Lagrangian dynamics is non-chaotic in spite of the strong chaoticity of the vortices and play an analogous role as coherent structures in two-dimensional turbulence [49].

It is known that around KAM tori periodic orbits of arbitrarily weak instability are present. These orbits are nearly marginally stable and cannot thus be considered hyperbolic.

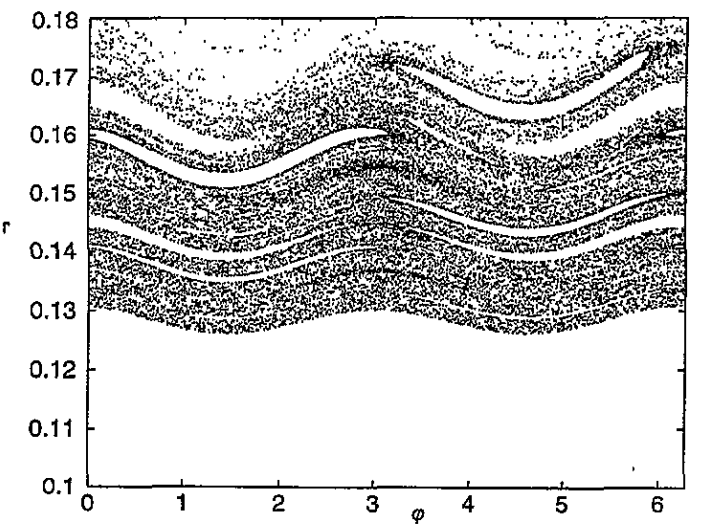

Figure 11. Magnification of the outer surface of the core of vortex 1, presented in polar coordinates r and φ. Although it looks rather smooth, many small tori are rolled up and seem to accumulate on the surface that is a KAM torus. The plot has been obtained by starting 200 trajectories on a small segment $\{0.63 < x < 0.7, y = 0.5\}$.

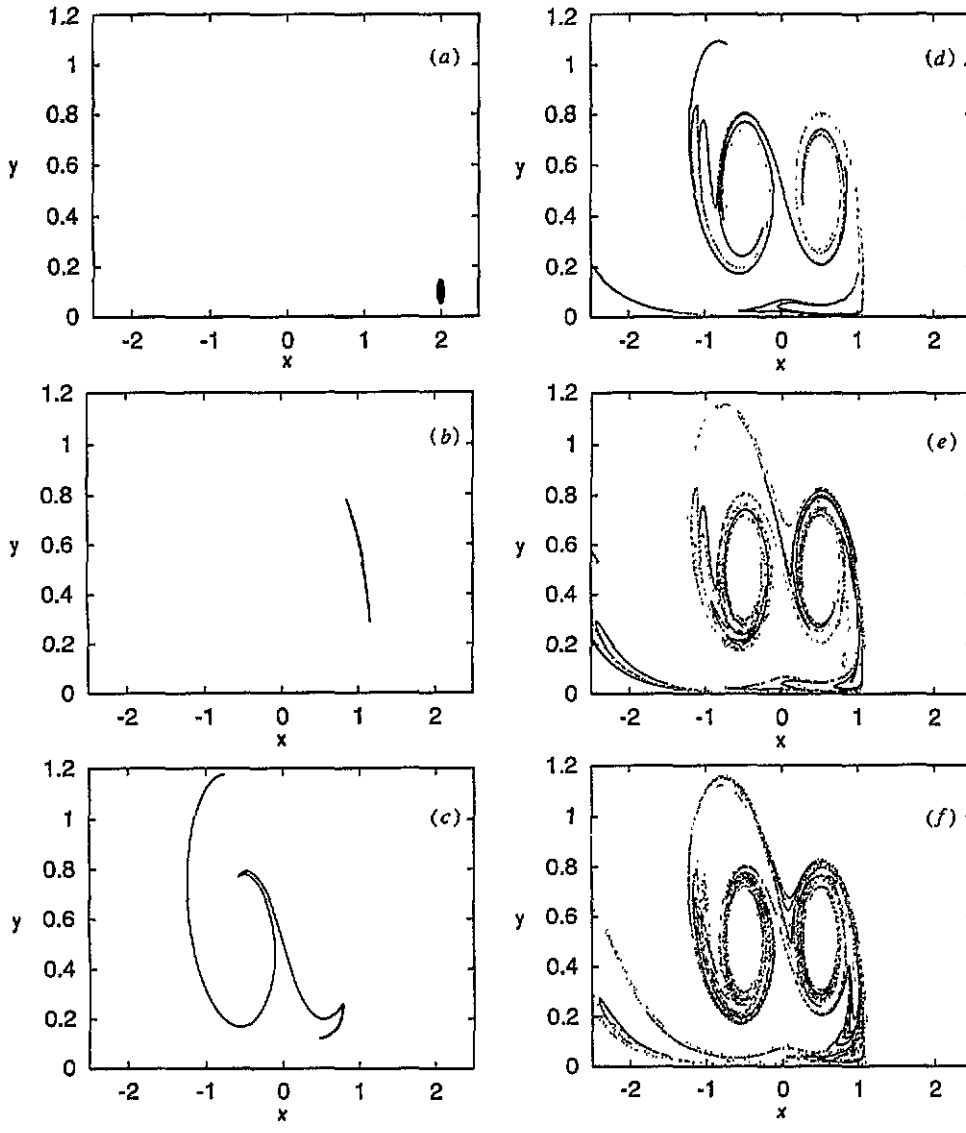

Figure 12. Motion of a droplet of dye particles on the stroboscopic plane in the CMS taken at $t = nT/2$ with $n = 0, \ldots, 5$ *(a)–(f).* 5×10^4 *tracer particles were started from a disc of radius* 0.05 centred at (2, 0.1). Observe that after only five time steps the ensemble of dye particles approaches the unstable manifold of the chaotic set very closely. This is always the case if the *set of initial conditions crosses the stable manifold of the chaotic set.*

Consequently, the component of the chaotic set lying around these KAM *tori will be called* the *non-hyperbolic component.* Due to the weak instability of the periodic orbits here (the stickiness of the tori), the decay from this region is rather slow, and the local structure of the set is dense, as being characterized by a fractal dimensionality close to unity [50].

The (un)stable manifold of the periodic point (P_2) P_1 is expected to come arbitrarily close to that of any other periodic orbit located in the unbounded part of the phase space. These manifolds together (more precisely, their closure) form the (un)stable manifold of

the chaotic set. In the CMS, the stable manifold at time t is mirror image with respect to the y-axis of the unstable one taken at $T/2 - t \bmod T/2$ (see equations (18), (19)). This equivalence of the manifolds is a consequence of the Hamiltonian character of the Lagrangian dynamics. Nevertheless, for the tracer particles the unstable manifold plays a distinguished role.

To see this, let us imagine that particles are injected into the flow in front of the vortex system. If the point of injection is not close to the x-axis or more generally to the stable manifold of the chaotic set, then the injected particles will not be trapped and will be advected away by the flow quite rapidly. Otherwise, however, the particle will be attracted, because of the stable foliation, to a vicinity of the chaotic set where it spends a finite amount of time, and escapes finally *along the unstable manifold of the chaotic set*. Therefore, we conclude that dye particles remaining for a long time around the vortex system will trace out the unstable manifold. This is consistent with recent results on chaotic advection in open flows [17, 19, 24, 28] showing that *streaklines* exhibiting fractal patterns asymptotically coincide with the unstable manifold of chaotic sets of the Lagrangian dynamics. (Streaklines [2, 30] are defined as sets of points reached, at a given instant of time, by a continuum of particles injected at a given point into the flow at any previous time before.) This is also an extension of the observations [5, 6, 8] obtained in closed flows claiming that dye particles move asymptotically along unstable manifolds of periodic orbits embedded in the chaotic sea.

In a series of pictures (figure 12) we present how a droplet of dye particles put into the flow in front of the vortex system evolves. It illustrates nicely the convergence toward the unstable manifold of the chaotic set. The shape of the structure traced out by the ensemble of droplet particles after time $t = 5T$ is given in figure 13 letting both the upper and lower half-planes and a few lobes from the tail of the chaotic set's unstable manifold be seen. The resemblance with the flow visualization picture of two leapfrogging vortex rings [30] is striking although the latter was made with three-dimensional rings in a real fluid.

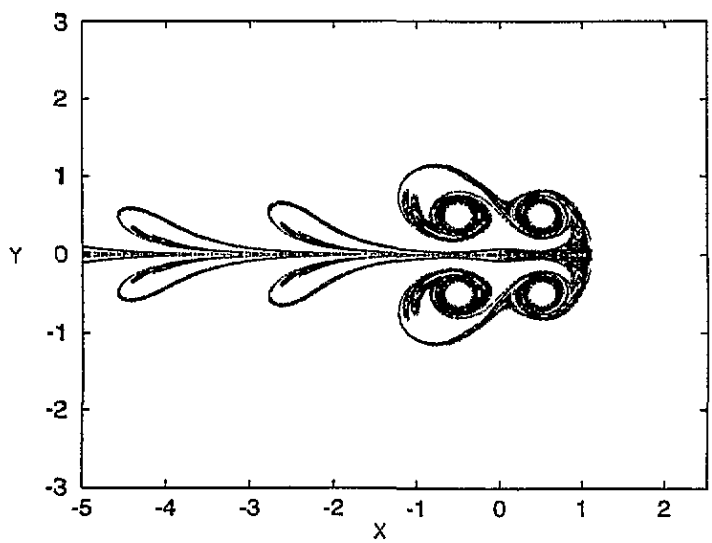

Figure 13. Unstable manifold of the full chaotic set in the CMS on large scale. The shape of the droplet at $t = 5T$ and its mirror image with respect to the x-axis are displayed. (In order to increase the density of points we plotted all images of the droplet points that remained in the region shown after $t = 5T$ up to at most $t = 60T$.) It has a similar form as the flow visualization pattern in an experiment with three-dimensional vortex rings [30].

5. The energy dependence

Up to this point we have focused our attention to the case of a given vortex energy $E = \ln 2$ which illustrated the basic features of the dynamics. By increasing the energy slightly further, the axisymmetric hyperbolic periodic orbit (V_1 and V_2 on the stroboscopic plane) becomes a *stable elliptic* one. In figure 14(a) we have plotted the unstable manifold of

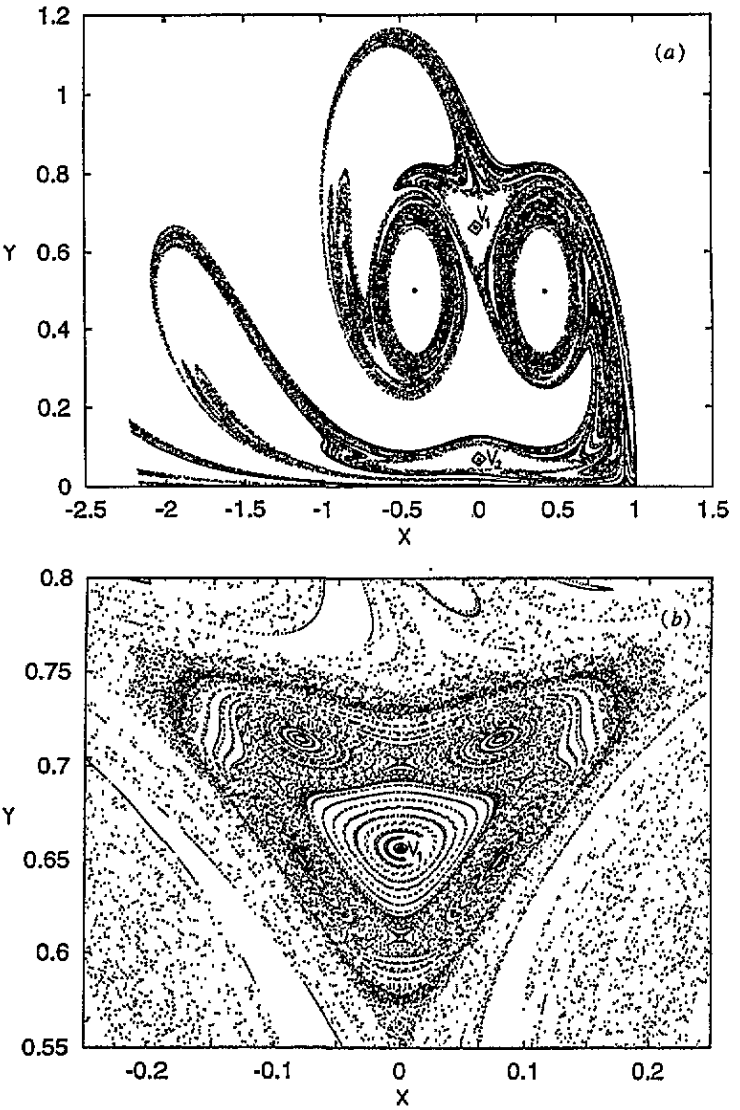

Figure 14. Invariant sets in the CMS for $E = \ln 2.5 = 0.916$ at $t = 0 \bmod T/2$. (a) Unstable manifold of the chaotic set obtained by using the droplet method with $t = 5T$ (cf figures 12 and 13). The fixed points V_1 and V_2 are now elliptic ones. (b) Magnification of the regular island near V_1. The plot has been obtained by starting 100 trajectories on the vertical segments $x = 0$ and $x = 0.075$, $0.55 < y < 0.8$, and plotting the first 200 iterates on the stroboscopic map. The vortex centres are marked by full circles.

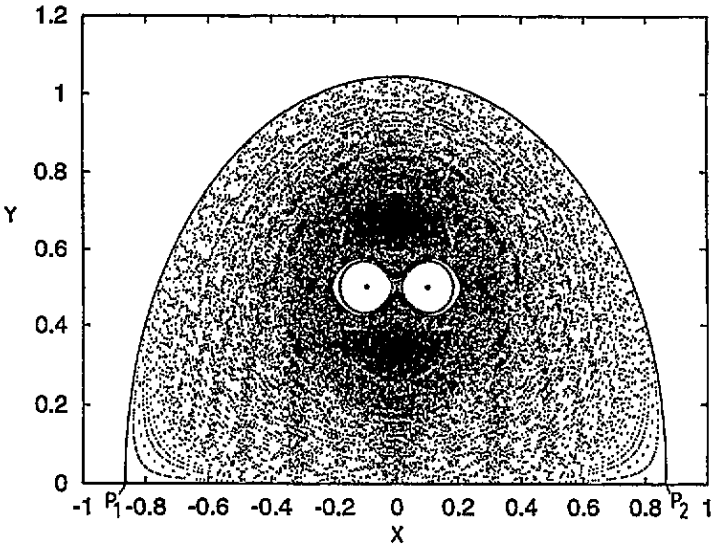

Figure 15. Invariant sets in the CMS for $E = \ln 25 = 3.21$ at $t = 0 \bmod T/2$. The unstable manifold (full curve) of the chaotic set is obtained by using the droplet method with $t = 5T$ (cf figure 12). Note that only a small part of the interaction region is available for scattering trajectories restricted to narrow regions of linear size of order 10^{-3} around $P_{1,2}$. The interior structure occupied by bounded trajectories have been visualized by starting 100 trajectories on the vertical line $x = 0$ and plotting the first 200 iterates on the stroboscopic map. The vortex centres are marked by full circles.

the chaotic set at $E = \ln 2.5$. One can observe two large islands around V_1 and V_2 and KAM tori on the boundary of them. The insides of these islands correspond to a bounded motion of the advected particles alternatively 'kicked' by the vortices. These regions are inaccessible by scattering trajectories and can only be seen by injecting particles inside of the vortex system. The structure of the phase space around the elliptic point V_1 is shown in figure 14(b). One can also clearly see the period-four stable periodic orbit just appeared, and the narrow bounded chaotic region around them. It would be interesting to check whether such bounded tracer motion could also be seen experimentally between two leapfrogging vortex rings.

By increasing the energy much further, bounded motion starts to dominate the dynamics. As an illustrative example we have plotted the unstable manifold of the chaotic set for $E = \ln 25$ (figure 15). Most of the central region is unaccessible by scattering trajectories. To illustrate this we have started 100 trajectories on the vertical line $x = 0$. One can clearly observe that besides the quasiperiodic motion there is also bounded chaotic motion in a layer close to the vortices. In addition to the large tori, many others show up on smaller scales which are either black or white regions in figure 15, depending on whether the $x = 0$ axis, where the trajectories start, intersects the tori (or their image).

Obviously the limiting case $E \gg 1$ corresponds to the advection in the field of a single vortex pair of strength 2 exposed to small periodic perturbation. The linear size of the region containing the two vortex cores and the two large KAM tori drastically shrinks with energy as it is of the order of $\exp(-E/2)$. Note, however, that the size of the interaction region is of order unity, also for $E \to \infty$. (The position of $P_{\pm}$, that is very close now to that of $P_{1(2)}$, is $x_{\pm} = \pm\sqrt{3}/2$ at any instant of time.) It is worth mentioning that the streamfunction in this

limit is similar to that of the oscillating vortex pair studied by Rom-Kedar *et al* [24]. The structural similarity of the two problems suggests that chaos in Melnikov's sense is present in the advection of leapfrogging vortices for $E \gg 1$ too, but its strength is diminishing as $E \to \infty$.

6. Quantitative characterization of the tracer dynamics

Early attempts to understand passive advection in the field of ideal vortices [24, 26] clearly reported about transient features of the dynamics. They gave a detailed characterization of escape but had difficulties in interpreting the motion as chaos because of the positivity of the Lyapunov exponent on finite time-scales only. Recent developments in the field of transient chaos [27] and chaotic scattering [20–22] help to overcome this difficulty by introducing the concept of natural measure on the non-attracting chaotic set, and the Lyapunov exponent taken with respect to this measure. The latter is thus a kind of ensemble average and is positive for transient chaos, too.

A central object in the theory of chaotic scattering [20–22] is the *time delay function* describing how the time spent in a region around the chaotic set depends on the initial conditions. In practice, one takes a one-parameter family of initial conditions and measures the number of periods the particle needs to leave a neighbourhood of the chaotic set as a function of the parameter. The time delay function of our model for $E = \ln 2$ is shown in figure 16. This function takes on an infinite value whenever the initial condition falls on the stable manifold of the chaotic set. These infinities thus appear in a fractal pattern. As the set of infinities is a kind of projection of the chaotic set along its stable manifold, the former has the same dimension d_0 as the partial dimension [52] of the chaotic set on the stroboscopic map.

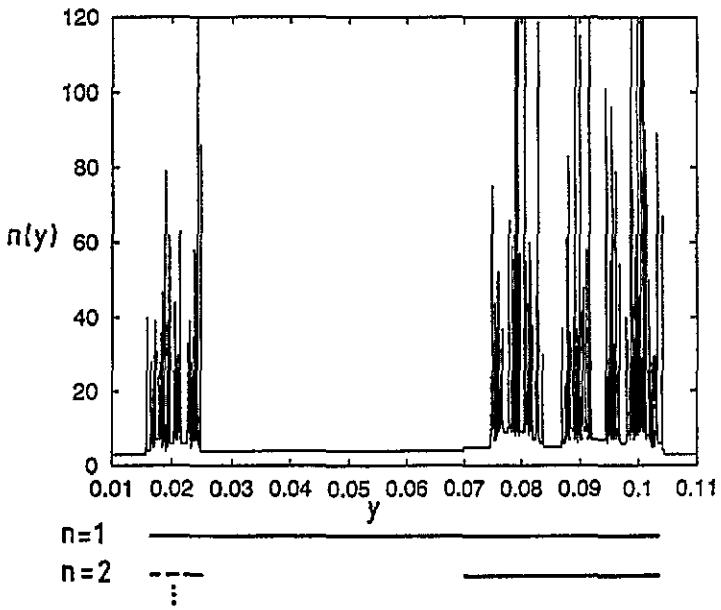

Figure 16. Time delay function $n(y)$ for $E = \ln 2$ where n is the number of periods $T/2$ spent in $|x| < 1.3$. Trajectories were started on the $x = 1.3$ line. The first two levels in the hierarchical organization are also shown.

In our numerical experiments 5×10^4 trajectories were started on a vertical line of length 0.1 at $x = 1.3$ with uniform distribution and we measured after how many time periods of $T/2$ they crossed the vertical line at $x = -1.3$. The well defined blocks of singularities in figure 16 correspond to the cross section of the initial line with the lobe E_{-2} (cf figure 9(*a*)). Since all these lobes are topologically similar, each of them contains the whole information about the dynamics and the investigation can be reduced to one of them.

Trajectories characterized by different time delay values mark different levels of a *hierarchy*. A quantity of central interest that reflects the hierarchical organization of chaotic scattering processes is the free energy $F(\beta)$. It characterizes the scaling behaviour seen by following trajectories with an increasing number n of periods inside the interaction region [51]. Let $l_i^{(n)}$ denote on each level n the length of intervals where the time delay function is greater or equal to $nT/2$ (see also figure 16). In the spirit of the thermodynamic formalism of dynamical systems [51], the free energy is defined via the relation

$$\sum_{i=1}^{N_0(n)} \left(l_i^{(n)}\right)^{\beta} \sim \mathrm{e}^{-\beta F(\beta) n} \tag{20}$$

where β is an arbitrary real number, $n \gg 1$, and $N_0(n)$ is the number of intervals at level n.

The escape rate α describes the exponential decay of the total interval length $\sum_i l_i^{(n)}$ with n. Thus,

$$\alpha = F(1)\,. \tag{21}$$

As long as no KAM tori are present or their role is not essential, α is non-zero, and $1/\alpha$ yields the average chaotic lifetime of scattering trajectories.

The topological entropy K_0 can be defined as the quantity characterizing the exponential growth of the number $N_0(n)$ of intervals with the level index n. Since the total number $N_0(n)$ of intervals is obtained from (20) at $\beta = 0$, we find

$$K_0 = -(\beta F(\beta))|_{\beta=0}\,. \tag{22}$$

Further important characteristics are the average Lyapunov exponent $\overline{\lambda}$ taken with respect to the natural measure, and the fractal dimension d_0 of the singularities in the time delay function. They can be obtained [51] as the derivative of $\beta F(\beta)$ taken at unity and as the value of β where the free energy vanishes, respectively, i.e. as

$$\overline{\lambda} = \frac{\mathrm{d}}{\mathrm{d}\beta}(\beta F(\beta))|_{\beta=1} \tag{23}$$

and

$$F(d_0) = 0\,. \tag{24}$$

In the presence of KAM surfaces, the distribution of trajectories staying for a given time in the interaction region decays more slowly than exponentially [50, 53] and the long-time behaviour is dominated by scattering trajectories staying close to the surface for long. Since the decay of the statistics, and of the total length of the scales $l_i^{(n)}$ is no longer exponential in n, both the escape rate and the average Lyapunov exponent should be zero in the asymptotic limit [54]. On general grounds one expects [50] that the fractal dimension tends to unity.

In figure 17 we have plotted the time delay statistics based on the time delay function of figure 16: the number of trajectories $N(n)$ with time delay larger or equal than a given number n times $T/2$. For $E = \ln 2$ a crossover between exponential and algebraic behaviour can be observed around $n \simeq 15$. For large n the scaling is algebraic due to the 'stickiness' of the tori, and we have found $N(n) \sim n^{-\sigma}$ with $\sigma \simeq 2$. Short orbits do not feel the

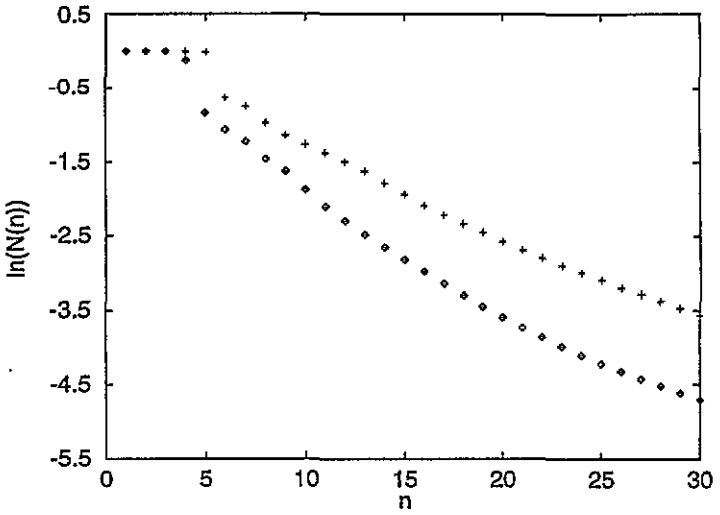

Figure 17. Time delay statistics for $E = \ln 2$ (diamonds) and $E = \ln 2.5$ (crosses). 5×10^4 trajectories have been started on the interval $x = 1.3, 0.01 \leqslant y \leqslant 0.11$. The number of trajectories $N(n)$ spending more time than $nT/2$ in the region $|x| < 1.3$ is shown on a log-linear plot. Observe the crossover around $n \simeq 15$ for $E = \ln 2$. For $n < 15$ the scaling is exponential with $\alpha \simeq 0.22$. For $E = \ln 2.5$ no well defined linear region can be seen.

influence of the tori and their scaling is governed by the hyperbolic part of the chaotic set. Indeed a well defined escape rate $\alpha = 0.22$ can be derived from the slope of the straight line for $n < 15$. The escape rate computed from the area of the lobes is nearly a factor 2 larger due to the crude approximation used there. It is worth noting, however, that for orbits started close to the outer surface of the vortex cores we have found a much slower algebraic decay in the time delay statistics with $\sigma \simeq 0.6$. This can be explained by the fact that typical scattering trajectories do not approach the vicinity of the core's surface. The core appears to be surrounded by a rather smooth surface that seems to be impenetrable for them, on finite time-scales at least.

For $E = \ln 2.5$ no exponential decay can be observed, the dynamics is dominated by non-hyperbolic effects. The algebraic decay exponent σ does not seem to depend strongly on the vortex energy.

In view of these observations we conclude that the computation of the free energy from the *low-lying levels* of the hierarchy enables us to obtain relevant information about the statistical properties of the *hyperbolic* component of the chaotic set as long as the energy is relatively small. So the results derived here are valid for not too long orbits (with time delay shorter than ~ 15 for $E = \ln 2$).

The free energy for $E = \ln 2$ computed from levels 4 and 5 is plotted in figure 18. For $\beta < 0$ the shortest intervals dominate the partition sum (20). Since the number of initial points influences essentially the resolution of the smallest intervals, for $\beta < 0$ one can observe a convergence with increasing number of trajectories. Although the free energy we obtained is not yet reliable for $\beta \leqslant 0$, in the range $\beta > \frac{1}{2}$ it seems to be converged. Thus we can read off the most important characteristics. For $E = \ln 2$ we thus obtain for the fractal dimension, the average Lyapunov exponent and the escape rate $d_0 = 0.83$, $\overline{\lambda} = 1.18$ and $\alpha = 0.22$, respectively. The topological entropy is $K_0 = 1.87$ with a relative error of $\sim 10\%$ due to the uncomplete convergence at $\beta = 0$.

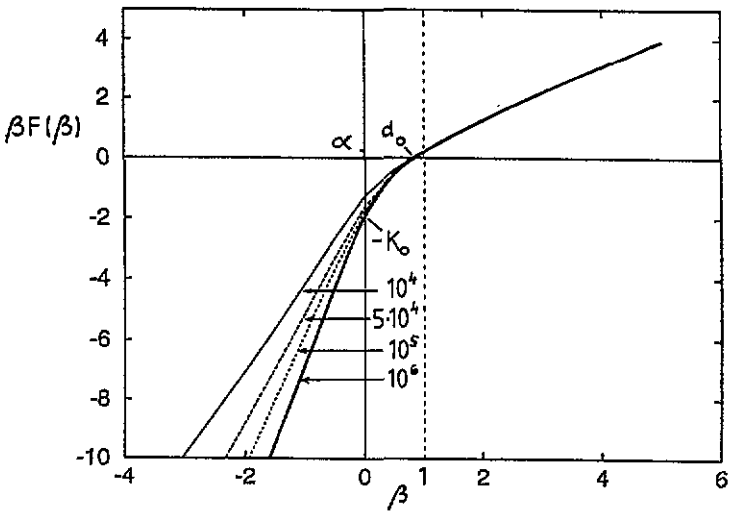

Figure 18. The free energy function as obtained from (20), from levels 4–5 for $E = \ln 2$. The convergence for $\beta < 0$ with increasing numbers of initial points 10^4, 5×10^4, 10^5 and 10^6 (taken on the interval $x = 1.3$, $0.01 \leqslant y \leqslant 0.11$) can also be seen.

The free energy $\beta F(\beta)$ is the Legendre transform of the multifractal spectrum $S(\lambda)$ of the *local Lyapunov exponents* λ [51]. Our results show that the latter spectrum can be obtained in a natural way by using the analogy with chaotic scattering, a method that is simpler than others based on directly following the deformation of material lines [55].

Since the chaotic set changes with energy, its properties also depend on this parameter. Larger energy implies smaller escape rate and larger fractal dimension. We have found that the approximate relation [56]

$$\overline{\lambda}(1 - d_0) \simeq \alpha \tag{25}$$

is satisfied in the energy range $0.4 < E < 0.9$ investigated. We also found that the average Lyapunov exponent does not change significantly, thus, the escape rate is proportional to $1 - d_0$. As the former was found to be a linear function of E in this range, we obtain

$$d_0 \simeq 0.83 + 0.2(E - \ln 2)\,. \tag{26}$$

We could not deduce any systematic change of the topological entropy due to the relatively large errors.

7. Concluding remarks

The advection problem in the time-periodic velocity field of two leapfrogging vortex pairs has been shown to comprise a variety of phenomena known to characterize different types of nonlinear systems. The invariant set can be divided into two parts depending on the boundedness of trajectories associated with it. One part is responsible for the motion of particles that never leave the vortex system. It certainly contains a component connected with bounded chaotic motion of tracer particles. The boundary of this part is formed by KAM tori. The other part of the invariant set is accessible by scattering trajectories belonging to particles injected into the flow far away from the vortices and exhibiting chaos on finite time-scales. It consists of a hyperbolic component the backbone of which is a fractal set

of strictly hyperbolic periodic orbits, and a non-hyperbolic one that is located close to the outer surface of the KAM tori. We claim that the coexistence of these different types of invariant sets is characteristic for general advection problems in open incompressible flows.

Whether bounded or scattering chaos dominates the tracer dynamics depends strongly on parameters of the flow, in our case on the total energy of the vortices. The latter is roughly speaking proportional to the compactness of the two-vortex-pair system. Our investigations showed that for loosely bounded pairs ($E < \ln 2$) it is hardly possible to find initial conditions numerically that lead to permanent chaos, and any kind of bounded motion can only be restricted to the cores of the vortices. At higher energies trajectories can be bounded in a region lying *between* the vortex pairs, too. Interestingly, the surface of KAM tori on the boundary of these regions seems to be rougher than that of the KAM tori on the boundary of the cores. Bounded chaos becomes more and more dominant with increasing energy while scattering chaos becomes suppressed. At even larger energies regular motion starts to characterize the problem since the limit $E \to \infty$ corresponds to so strongly bounded vortex pairs that they can be approximately replaced by one single pair. The advection problem is integrable in this limit.

The scenario briefly sketched above contains open problems that could be subjects of further studies. It is not yet completely understood how the strongly hyperbolic axisymmetric orbit will be elliptic in a narrow range of energies (between $E = 0.7$ and 0.9). Its bifurcation diagram, as well as of other periodic orbits, could be interesting to follow with the energy.

We have not yet mentioned what happens to the advection dynamics at very low energies. Our results show that the overall qualitative picture is similar to that found at $E = \ln 2$, the quantitative characteristics, however, change drastically for $E \to +0$. In particular, the escape rate and the average Lyapunov exponent seem to diverge in this limit, while the fractal dimension seems to tend to zero. This raises the question of what happens when crossing the line $E = 0$ from the side of negative energy values where the vortex motion is not bounded. It is possible that a chaotic set will be created suddenly at $E = 0$ very much in the same spirit as in the course of abrupt bifurcations [57]. This, however, can only hold for the hyperbolic component. The entire process should be more complicated due to the presence of KAM tori around the cores, and certainly deserves further attention.

Acknowledgments

One of us (TT) is deeply indebted to L Sasvári for introducing him to the problem of vortex dynamics and for several valuable discussions. Useful comments of S Jones, O Piro, A Provenzale and L Zannetti are acknowledged. We thank Gy Károlyi and K G Szabó for a critical reading of the manuscript. This work was partially supported by the Hungarian Science Foundation under grant nos OTKA 2090, T4439, F4286, by the Foundation for Hungarian Higher Education and Research, and by the PHARE ACCORD Program H9112-0378.

Appendix. The equations of the vortex dynamics

Introducing the coordinates x_0, x_r and $2y_0$, $y_r/2$ of (5), (6) and (8) as new variables, that corresponds to a canonical transformation, the Hamiltonian (4) reads as

$$H(x_0, x_r, 2y_0, y_r/2) = \tfrac{1}{2} \ln \frac{(x_r^2 + (2y_0)^2)((2y_0)^2 - 4(y_r/2)^2)}{x_r^2 + 4(y_r/2)^2}. \tag{A1}$$

The equations of motion are obtained in the form

$$\dot{x}_r = -2y_r \frac{(2y_0)^2 + x_r^2}{((2y_0)^2 - y_r^2)(x_r^2 + y_r^2)} \tag{A2}$$

$$\dot{y}_r = 2x_r \frac{(2y_0)^2 - y_r^2}{((2y_0)^2 + x_r^2)(x_r^2 + y_r^2)} \tag{A3}$$

$$\dot{x}_0 = 2y_0 \frac{x_r^2 - y_r^2 + 2(2y_0)^2}{((2y_0)^2 - y_r^2)((2y_0)^2 + x_r^2)} \tag{A4}$$

$$\dot{y}_0 = 0\,. \tag{A5}$$

Choosing the conserved coordinate $2y_0$ as the length scale l (7) formally means replacing $2y_0$ by 1. The first two equations form a closed system and can be integrated numerically to describe the relative motion of the vortices. The third equation (A4) gives the net translational motion of the centre-of-mass coordinate.

Using equations (A2) and (9),

$$\mathrm{d}t = -\frac{A}{2} \frac{[1 - y_r^2(x_r)]^2}{y_r(x_r)} \mathrm{d}x_r \tag{A6}$$

follows, where $A \equiv \mathrm{e}^{-E}$. The functional form of $y_r(x_r)$ is given by (9) as

$$y_r = \gamma^{-1} \left(\frac{\gamma^2 - x_r^2}{\beta^2 + x_r^2} \right)^{1/2} . \tag{A7}$$

Here we have used the abbreviations $\gamma \equiv \sqrt{A/(1-A)}$, and $\beta \equiv \sqrt{(1+A)/A}$. From equation (9) one easily sees that the trajectory is symmetric to the axes $x_r = 0$ and $y_r = 0$, and therefore it is sufficient to integrate (A6) from $x_r = 0$ to the maximum value γ of x_r which corresponds to a quarter of a period. Thus for the period T follows

$$T = 2A \int_0^\gamma \frac{[1 - y_r^2(x_r)]^2}{y_r(x_r)} \mathrm{d}x_r\,. \tag{A8}$$

This can be written as the sum of three terms:

$$T = 2A(S_1 - 2S_2 + S_3) \tag{A9}$$

with

$$S_i = \int_0^\gamma [y_r(x_r)]^{\sigma_i} \mathrm{d}x_r \tag{A10}$$

$$= \gamma^{-\sigma_i} \int_0^\gamma \left(\frac{\gamma^2 - x_r^2}{\beta^2 + x_r^2} \right)^{\sigma_i/2} \mathrm{d}x_r \tag{A11}$$

where $\sigma_i = 2i - 3$ $(i = 1, 2, 3)$. These quantities can be expressed in terms of elliptic integrals [58]. Inserting S_i we find for the period T:

$$T = \frac{4}{A} \left[\frac{1}{1 - A^2} \boldsymbol{E}(A) - \boldsymbol{K}(A) \right] \tag{A12}$$

where $\boldsymbol{K}(A)$ and $\boldsymbol{E}(A)$ are the complete elliptic integrals of first and second type, respectively. Using the asymptotic expansion of these elliptic integrals for $A \ll 1$ [58], we find in the high-energy limit ($E \gg 1$) that the period can be expressed as

$$T \sim \pi \mathrm{e}^{-E} + \frac{9\pi}{8} \mathrm{e}^{-3E} + \cdots . \tag{A13}$$

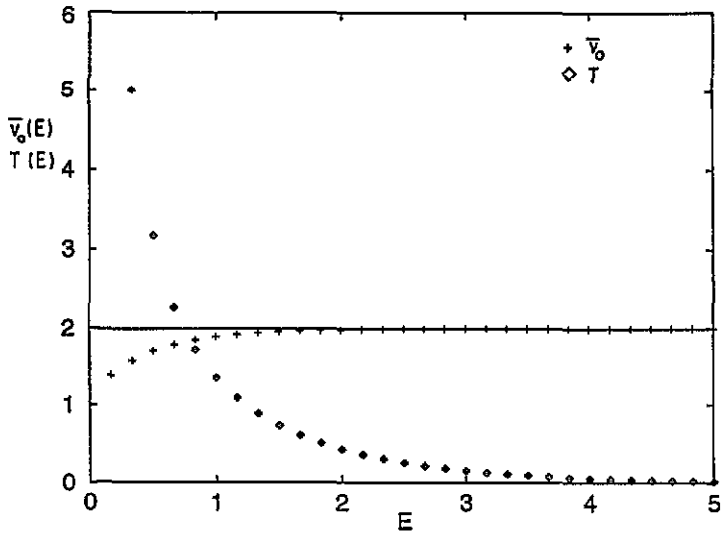

Figure A1. The period T (diamonds) and the average velocity $\overline{v}_0$ (crosses) of the leapfrogging motion of the vortex pairs as a function of energy E (cf equations (A12) and (A16) where $A = e^{-E}$).

Analogously, one can obtain the energy dependence of the mean velocity

$$\overline{v}_0 = \frac{1}{T}\int_0^T \dot{x}_0(t)\,dt\,. \tag{A14}$$

Using equation (9), (A4) takes the form

$$\dot{x}_0 = \frac{2}{1-y_r^2} - A\,. \tag{A15}$$

By means of (A6) and (A10) we obtain

$$\overline{v}_0 = A\left(4\frac{S_1 - S_2}{T} - 1\right). \tag{A16}$$

Proceeding similarly as for the period, finally one finds

$$\overline{v}_0 = \frac{A^2 E(A)}{E(A) - (1-A^2)K(A)}\,. \tag{A17}$$

The functions $T(E)$ and $\overline{v}_0(E)$ are plotted in figure A1. Observe that even at relatively small energies ($E > \ln 2$) the mean velocity is practically independent of E. Using the series expansions for elliptic integrals one obtains

$$\overline{v}_0 \sim 2 - \tfrac{3}{4}e^{-2E} + \cdots \tag{A18}$$

implying that the saturation value 2 is reached exponentially fast with increasing energies.

References

[1] Ottino J M 1989 *The Kinematics of Mixing: Stretching, Chaos and Transport* (Cambridge: Cambridge University Press)
[2] Ottino J M 1990 *Ann. Rev. Fluid. Mech.* **22** 207
[3] Crisanti A, Falcioni M, Paladin G and Vulpiani A 1991 *Riv. Nuovo Cimento* **14** 1
[4] Wiggins S 1992 *Chaotic Transport in Dynamical Systems* (Berlin: Springer)

[5] Aref H and Balachandar S 1986 *Phys. Fluids* **29** 3515
[6] Chaiken J, Chevray R, Tabor M and Tan Q M 1986 *Proc. R. Soc.* A **408** 165
[7] Feingold M, Kadanoff L P and Piro O 1988 *J. Stat. Phys.* **50** 529
[8] Muzzio F J, Swanson P D and Ottino J M 1992 *Int. J. Bifurc. Chaos* **2** 37
Jana S C, Metcalfe G and Ottino J M 1994 *J. Fluid Mech.* **269** 199
[9] Ouchi K *et al* 1991 *Prog. Theor. Phys.* **85** 687
Ouchi K and Mori H 1992 *Prog. Theor. Phys.* **88** 467
[10] Solomon T H and Gollub J P 1988 *Phys. Rev.* A **38** 6280
Solomon T H, Weeks E R and Swinney H L 1993 *Phys. Rev. Lett.* **71** 3975; 1994 *Physica* **76D** 70
[11] Chernikov A A and Schmidt G 1992 *Phys. Lett.* **169A** 51
[12] Sommerer J C and Ott E 1993 *Science* **259** 281
Sommerer J C 1994 *Physica* **76D** 85
[13] Jones S and Aref H 1988 *Phys. Fluids* **31** 469
[14] Jones S, Thomas O and Aref H 1989 *J. Fluid. Mech.* **116** 335
[15] Young W R and Jones S 1991 *Phys. Fluids* A **3** 1087
[16] Pierrehumbert R T 1991 *Phys. Fluids* A **3** 1250
Brown M G and Smith K B 1991 *Phys. Fluids* A **3** 1187
[17] Shariff K, Pulliam T H and Ottino J M 1991 *Lect. Appl. Math.* **28** 613
[18] Jung C and Ziemniak E 1992 *J. Phys. A: Math. Gen.* **25** 3929
Jung C, Tél T and Ziemniak E 1993 *Chaos* **3** 555
[19] Ziemniak E, Jung C and Tél T 1994 *Physica* **76D** 123
Jung C and Ziemniak E 1994 *Fractals in the Natural and Applied Sciences* ed M M Novak (Amsterdam: North-Holland)
[20] Smilansky U 1992 *Chaos and Quantum Physics* ed M J Giannoni *et al* (New York: Esevier)
[21] Jung C 1992 *Acta. Phys. Pol.* **23** 177
[22] Ott E and Tél T 1993 *Chaos* **3** 417
[23] Aref H 1983 *Ann. Rev. Fluid. Mech.* **15** 345; 1984 *J. Fluid. Mech.* **143** 1
[24] Rom-Kedar V, Leonard A and Wiggins S 1990 *J. Fluid. Mech.* **214** 347
[25] Shoutherland K B, Porter J R III, Dahm W J A and Buch K A 1991 *Phys. Fluids* A **3** 1385
van Heijst G J F and Flór J B 1989 *Nature* **340** 212
Carnevale G F, Kloosterziel R C and van Heijst G J F 1991 *J. Fluid. Mech.* **233** 119
Auerbach D 1991 *Phys. Fluids* A **3** 1351
Carnevale G F and Kloosterziel R C 1994 *Physica* **76D** 147
[26] Zawadzki I and Aref H 1991 *Phys. Fluids* A **3** 1405
Meleshko V V, Yu Konstantinov M, Gurzhi A A and Konovaljuk T P 1992 *Phys. Fluids* A **4** 2779
Meleshko V V and van Heijst G J F 1994 *Chaos, Solitons & Fractals* **4** 977; 1994 *J. Fluid Mech.* **272** 157
[27] Tél T 1990 *Directions in Chaos* ed Hao Bai-Lin vol 3 (Singapore: World Scientific) pp 149–221
[28] Shariff K, Leonard A, Zabusky N J and Ferziger J H 1988 *Fluid. Dynam. Res.* **3** 337
[29] Shariff K 1989 *PhD Thesis* Stanford University
Shariff K, Leonard A 1992 *Ann. Rev. Fluid. Mech.* **24** 235
[30] Yamada H and Matsui T 1978 *Phys. Fluids* **21** 292
Van Dyke M 1982 *An Album of Fluid Motion* (Stanford: Parabolic) p 46
[31] Lamb H 1932 *Hydrodynamics* (Cambridge: Cambridge Unoversity Press)
[32] Kochin N E, Kibel I A and Rose N V 1964 *Theoretical Hydrodynamics* (New York: Interscience)
[33] Saffman P G 1992 *Vortex Dynamics* (Cambridge: Cambridge University Press)
[34] Novikov E A and Sedov Yu B 1978 *Sov. Phys.–JETP* **48** 440
[35] Aref H and Pomphrey N 1982 *Proc. R. Soc.* A **380** 359
[36] Zannetti L and Franzese P 1993 *Euro. J. Mech. B/Fluids* **12** 43; 1994 *Physica* D **76** 99
[37] Kadtke J B *PhD Thesis* Brown University
Okamoto H and Kimura Y 1989 *Topological Fluid Mechanics* ed H K Moffat and Tsinober (Cambridge: Cambridge University Press) pp 105–13
Meleshko V V 1994 *Phys. Fluids* **6** 6
[38] Eckhardt B and Aref H 1988 *Phil. Trans. R. Soc.* A **326** 655
Echardt B 1988 *Europhys. Lett.* **5** 107
Aref H, Jones S W, Mofina S and Zawadski I 1989 *Physica* **37D** 423
[39] Eckhardt B 1988 *Phys. Fluids* **31** 2796
[40] Rott N 1990 *Phys. Fluids* A **2** 1477
[41] Kadtke J B and Novikov E A 1993 *Chaos* **3** 543

[42] Chapman D 1978 *J. Math. Phys.* **19** 1988
[43] van Kempis A and Lustfeld H 1993 *J. Phys. A: Math. Gen.* **26** 261
[44] Beigie D, Leonard A and Wiggins S 1991 *Phys. Fluids* A **3** 1039
Camassa R and Wiggins S 1991 *Phys. Rev.* A **43** 774
Weiss J B and Knobloch E 1989 *Phys. Rev.* A **40** 2579
Weiss J B 1994 *Physica* **76D** 230
[45] Nusse H E and Yorke J 1989 *Physica* **36D** 137
[46] Kovács Z and Wiesenfeld L 1995 Chaotic scattering in reactive collisions: a classical analysis *Phys. Rev.* E at press
[47] Guckenheimer J and Holmes P 1983 *Nonlinear Oscillations, Dynamical Systems, and Bifurcations of Vector Fields* (Berlin: Springer)
[48] Babiano A, Boffetta G, Provenzale A and Vulpiani A 1994 *Phys. Fluids* A **6** 2465
[49] Elhmaidi D, Provenzale A and Babiano A 1993 *J. Fluid. Mech.* **257** 533;
Provenzale A, Babiano A and Villone B 1994 Single-particle trajectories in two-dimensional turbulence *Chaos Solitons & Fractals* at press
[50] Lau Y T, Finn J M and Ott E 1991 *Phys. Rev. Lett.* **66** 978
[51] Kovács Z and Tél T 1990 *Phys. Rev. Lett.* **64** 1617
[52] Grassberger P and Procaccia I 1984 *Physica* **13D** 34
[53] Ding M, Bountis T and Ott E 1990 *Phys. Lett.* **151A** 395
[54] Christiansen F and Grassberger P 1993 *Phys. Lett.* **181A** 47
[55] Vulpiani A 1989 *Physica* **38D** 372
Városi F, Antonsen T M Jr and Ott E 1991 *Phys. Fluids* A **3** 1017
Beigie D, Leonard A and Wiggins S 1993 *Phys. Rev. Lett.* **70** 275
Gallucio S and Vulpiani A 1994 *Physica* **212A** 75
[56] Kantz H and Grassberger P 1985 *Physica* **17D** 75
[57] Bleher S, Grebogi C and Ott E 1989 *Phys. Rev. Lett.* **63** 919; 1990 *Physica* **46D** 87
[58] Ryshik I M and Gradstein I S 1957 *Tables of Series, Products, and Integrals* (Berlin: Springer)